Characterization of Re-Ni Films after the Initial Stages of Electrodeposition

O. Berkh,[a] L. Burstein,[b] A. Gladkikh,[b] N. Eliaz,[c,*,z] and E. Gileadi[d,]**

[a]*Department of Physical Electronics, School of Electrical Engineering, Tel Aviv University, Ramat Aviv 6997801, Israel*
[b]*Wolfson Applied Materials Research Center, Tel Aviv University, Ramat Aviv 6997801, Israel*
[c]*Department of Materials Science and Engineering, Tel Aviv University, Ramat Aviv 6997801, Israel*
[d]*School of Chemistry, Tel Aviv University, Ramat Aviv 6997801, Israel*

Re-Ni layers produced in the early stages of electrodeposition from citrate electrolytes were studied by high-resolution X-ray photoelectron spectroscopy (HR-XPS) and time-of-flight secondary-ion mass spectrometry (TOF-SIMS). The deposition time was varied in the range of 2 to 300 seconds. The compositional heterogeneity of the thin Re-Ni alloys and the variations of their composition with deposition time, both in the bulk and on the surface, were shown. The results obtained are indicative of the occurrence of chemical reactions at short deposition times and are in agreement with our previous results obtained in studying the early stages of Re-Ni deposition by electrochemical techniques. The mechanism of the deposition process is discussed.
 [DOI: 10.1149/2.0631607jes]

Manuscript submitted January 5, 2016; revised manuscript received April 4, 2016. Published April 16, 2016.

Induced electrodeposition of refractory metals with iron-group metals has drawn the attention of many researchers in view of their high corrosion resistance, stability at high temperatures and wear resistance.[1] Induced codeposition of rhenium from aqueous solutions has been studied,[2–5] including Re-Ni alloys from citrate-containing solutions.[6–9]

Induced codeposition of Re from an electrolyte containing ReO_4^- can occur readily. Coatings with a thickness of up to 25 μm were obtained within 60 min deposition at a faradaic efficiency of up to 95%. Moreover, the concentration of Re in the resulting alloy can reach up to 90 at.%. This excludes the possibility of having a precursor similar to that found in the case of W,[1,10–12] since it would require the formation of a complex containing nine molecules of the perrhenate ion, which is totally unlikely. Instead, we have suggested a new mechanism, according to which the Ni^{2+} ion is first reduced and deposited on the surface of the substrate. The resulting neutral Ni atoms act as strong reducing agents, helping to reduce the 7-valent ReO_4^- probably to the 5-valent ReO_3^-. This is a typical catalytic process, in which the Ni^{2+} ion acts as a catalyst, the concentration of which should not change in the overall reaction. Theoretically, this should lead to a deposit of pure Re, but some Ni is found in the resulting alloy due to entrapment of neutral Ni atoms. This represents a rather unique type of process, where the catalyst is formed in situ as part of the redox process.[6–9] The deposition of Re-Ni apparently depends on the high catalytic activity of the freshly deposited nickel. We have supported this hypothesized mechanism by different experiments.[7,13–15]

The initial stages of Re-Ni deposition, which are critical for understanding the catalytic mechanism, were studied in our recent work.[13] There, the electrodeposition of Re-Ni alloys was investigated at deposition times of 0.05–60 s, unlike in earlier publications,[6–8] where the deposition times were on the scale of minutes and hours. The anomalous faradaic efficiency (AFE) of the deposition process, the composition of the deposits and their morphology were considered. The AFE and the Re-content in the deposits were shown to decrease with deposition time. Anomalous values of the AFE, well above 100%, were observed at short deposition times. This indicates some chemical reactions occurrence in parallel with the electrochemical charge transfer process, in the early stages of deposition. A decline in the rate of the chemical reaction, leading to the decrease of the AFE and a decline of the Re-content in the deposit, was interpreted as change in the catalytic properties of the surface of the cathode during deposition.[13] The effects of current density, electrolyte composition, stirring and pH on the initial stages of deposition were studied too.[13,14]

Re-Ni citrate electrolytes of different compositions were studied by Raman spectroscopy.[14] Peaks of two fundamentals of ReO_4^-, at 972 cm^{-1} and at 331 cm^{-1}, were attributed to symmetric stretching of the Re=O and deformation of O-Re-O, respectively. The ratio of these peak intensities was shown to decrease with the concentration of Ni ions and the ratio of Ni/Re ions in the electrolyte. The effect of Ni-Cit ions on atom oscillations in ReO_4^- designates ReO_4^- ion deformation. Therefore, on the basis of these results we speculated some interaction of Ni-Cit ions with ReO_4^-, leading to their deformation. The interaction was assumed to be weak since no shift of the fundamental positions was observed. Additionally, no complexes of ReO_4^- and Ni ions in citrate electrolytes were observed by UV-Vis spectroscopy and conductometry. Recently, we have further supported the suggested mechanism experimentally, employing spherical aberration-corrected scanning transmission electron microscopy (STEM) and atom-probe tomography (APT) to characterize the atomic-scale structure and atomic part-per-million level three-dimensional chemistry of a Re-Ni coating. A unique combination of a multilayer and columnar Re-Ni structure was observed, consisting of thicker Re-rich and thinner Ni-rich alternating layers.[15]

In the current work, we used Time-of-Flight Secondary-Ion Mass Spectrometry (TOF-SIMS) and High-Resolution X-Ray Photoelectron Spectroscopy (HR-XPS) for studying the Re-Ni deposits produced in the initial stages of deposition. The results obtained confirm the concept of chemical reaction fading with increasing deposition time, and are in agreement with the compositional changes of the catalytic electrode surface during the Re-Ni deposition process.

Experimental

Re-Ni alloys for HR-XPS and TOF-SIMS analysis were deposited galvanostatically at 50 mA cm^{-2} in stirred electrolytes containing 94 mM nickel sulfamate, 34 mM ammonium perrhenate, and 100 mM citric acid. The pH of the electrolytes was adjusted to 5.0 ± 0.1 by addition of 5.0 M NaOH. The bath temperature was held at 70 ± 1°C.

TOF-SIMS was applied to detect species incorporated in the Re-Ni deposits. A TRIFT-II model TOF-SIMS spectrometer from Physical Electronics was used. The TOF-SIMS depth profiles were measured with positive ions, using 2 keV O_2^+ sputter beam and 15 keV Ga^+ analytical ion beam. Surface mass spectra and depth profiles were studied for Re-Ni deposits produced at 2, 5, 10, 15, and 20 s. Deposition was conducted on 0.5 cm^2 Si substrates with native oxide, on which 20 nm Ti adhesion layer and 100 nm Au conductive layer were sputtered.

XPS measurements were performed in ultrahigh vacuum (2.5×10^{-10} Torr base pressure), using a 5600 Multi-Technique system (PHI, MN). The samples were irradiated with an Al-Kα monochromatic

*Electrochemical Society Member.
**Electrochemical Society Fellow.
[z]E-mail: neliaz@tau.ac.il

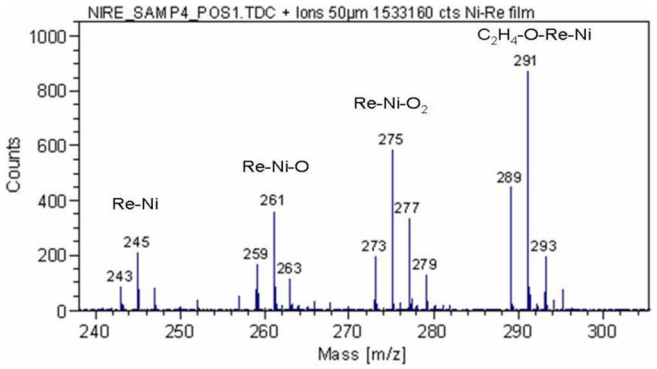

Figure 1. TOF-SIMS spectrum of the surface of electrodeposited Re-Ni alloy.

source (1486.6 eV), and the outcome electrons were analyzed by a spherical capacitor analyzer using a slit aperture of 0.8 mm in diameter. The samples were not charged during measurements. They were analyzed at the surface and after sputter cleaning using 4 kV Ar^+ ion gun (the sputter rate was about 4.8 nm min^{-1} on SiO_2/Si reference sample). High-resolution spectra were taken at pass energy of 11.75 eV at increments of 0.05 eV $step^{-1}$ to allow precise energy positioning and peak shape determination. All peaks were referenced to C1s peak position at 285 eV. Curve fitting was done with Gaussian-Lorentzian function using the 5600 Multi-Technique System software. HR-XPS spectra were analyzed for the Re-Ni deposits produced on 0.5 cm^2 Pt foil electrodes for 5, 10, 20, or 300 s.

Results and Discussion

TOF-SIMS analyses.—Typical mass spectra of the surface in the range of 238–345 m/z are shown in Fig. 1. The surface mass spectra indicate the presence of Re-Ni, Re-Ni-O_x (Re-Ni-O, Re-Ni-O_2) and C_2H_4-O-Re-Ni species (along with Ni, Re, NiO_x, ReO_x species, which are not shown here). SIMS profiles for the films deposited for 2, 5, 10, 15 and 20 s are presented in Figs. 2a–2e, respectively. The secondary-ion intensity depends on the ionization yields of the sputtered atoms of an element and on their chemical state in the sputtered material. These effects make SIMS difficult to apply to the quantitative analysis of the alloy components.[16] However, the SIMS profile allows observation of the composition changes through the film depth.

Analysis of the SIMS profiles (cf. Fig. 2) reveals the following effects:

(i) Re-Ni ions were detected along with separate Ni and Re ions, for all investigated deposits.
(ii) Secondary-ion intensity for Ni increased noticeably from the substrate/deposit interface to the outer surface of Re-Ni deposits. This trend corresponds to the decrease of Re concentration with deposition time, and is consistent with the EDS analysis of the films.[13] Along with this, a small periodic increase and decrease of Ni ion intensity with sputtering time can be seen.
(iii) Periodic changes of Re and Re-Ni ion intensities with sputtering time were observed. The increase of the Re and Re-Ni intensities are accompanied by the decrease of Ni intensity, and vice versa.

The thickness of the Re-Ni deposits was determined based on weight gain measurements ($t = 300$ s deposition time under the given conditions yields a deposit thickness of 2,500 nm, with a FE of about 95%). We calculated the thickness values h_1 for different deposition times using Eq. 1, in which the units of h_1 and t are nm and s, respectively. The corresponding values of the FE were determined by anodic stripping:[13]

$$h_1 = (2,500 \times t \times \mathrm{FE}) / (300 \times 95) \qquad [1]$$

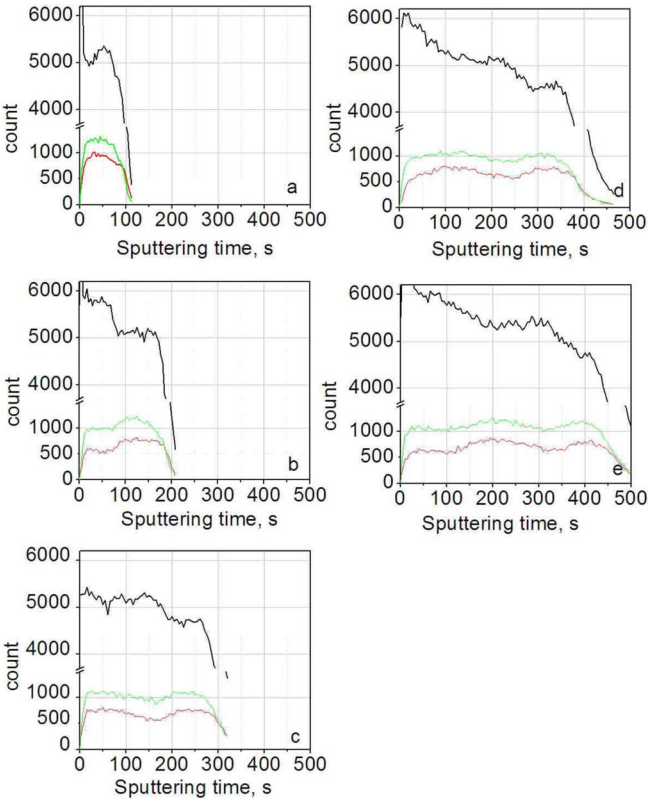

Figure 2. SIMS depth profiles of Re, Re-Ni and Ni signals for Re-Ni deposits formed at 2 s (a), 5 s (b), 10 s (c), 15 s (d) and 20 s (e); red – Re, black – Ni, green – Re-Ni.

The thickness of the Re-Ni deposits (h_2) was also calculated for every deposition time using Eq. 2, in which the units of h_2, sputtering rate and sputtering time are nm, nm s^{-1} and s, respectively. The sputtering time (proportional to the film thickness) for every deposit was taken at the position corresponding to the drop of count by 50% (Fig. 2). The sputtering rate was estimated to be about 0.39 nm s^{-1}. The thickness values evaluated by both electrochemical and SIMS techniques for different deposition times are very close (see Table I).

$$h_2 = \text{sputtering rate} \times \text{sputtering time} \qquad [2]$$

Figure 3 shows the sputtering time and charge density Q (in units of C cm^{-2}) vs. the deposition time. The charge density was calculated using anodic stripping voltammograms.[13] The dependences are almost linear ($R^2 = 0.99$ and 0.98 for t and Q, respectively). Extrapolation of the straight lines for the charge density and sputtering time to zero time crosses the ordinate significantly above zero. This finding is consistent with the observations found using anodic stripping, showing that chemical reactions are also observed in parallel with the electrochemical reactions.[13] The data in Fig. 3 indicate consistency between the SIMS and the electrochemical measurements. Thus, SIMS results

Table I. Deposit thickness values estimated by electrochemical and SIMS methods. Sputtering rate = h_1 / sputtering time = 39/100 = 0.39 nm s^{-1}. Deposition time $t = 2$ s.

Deposition time (s)	Sputtering time (s)	FE, Ref. 13	h_1 (nm), based on weight gain[13]	h_2 (nm), based on sputtering rate
2	100	220	39	39
5	190	178	78	74
10	303	140	123	118
15	388	110	145	151
20	466	105	184	182

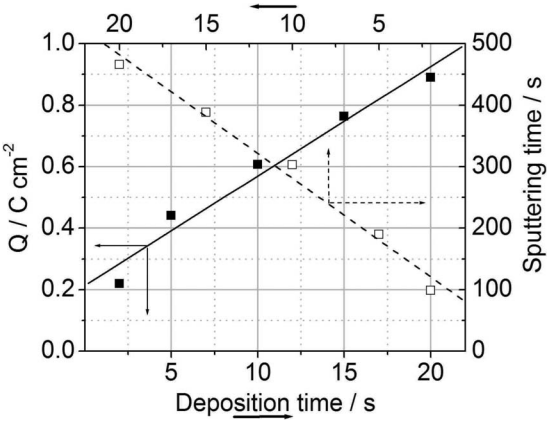

Figure 3. The effect of deposition time on the specific anodic stripping charge density that represents the amount of deposited material and on the SIMS sputtering time that represents the thickness of deposits.

confirm the high deposition rates and the corresponding AFE at short deposition times, followed by the decrease of the AFE with increasing deposition time, as reported before.[13] Data of sputtering time and film thickness vs. electrodeposition time (Table I and Fig. 3) is consistent with the occurrence of a chemical process that slows down with increasing deposition time.

HR-XPS analyses.—HR-XPS spectra were analyzed for the Re-Ni films deposited at 50 mA cm^{-2} and 70°C for 5, 10, 20 and 300 s. Typical HR-XPS Re 4f and Ni 2p spectra are shown in Figs. 4a and 4b, respectively. The HR-XPS Re 4f and Ni 2p spectra obtained before and after sputter cleaning are very different. No metal oxides are observed after 1 min sputtering of the film surface.

Tables II and III summarize the results of curve fitting for non-sputtered Re-Ni films deposited at different times. Data presented in Table II have been recalculated without satellites. As shown in these tables, the fitted spectra before sputtering contain both metallic and oxidized species. Re 4f component attribution is in agreement with published data on Re,[17] Re-Ni,[7] ReO_2,[18] Re_2O_5,[7] ReO_3,[18] and ReO_4^-.[18] Binding energies of oxidized components in the Ni $2p_{3/2}$ fitted structure suggest the existence of NiO at 853.91–854.11 eV,[19–21] and $Ni(OH)_2$ at 856.3 eV,[20] where the latter can also be attributed to some nickel-citrate complexes resulting from the presence of citrate in solution. Non-oxidized Ni $2p_{3/2}$ peak position (852.87–853.07 eV) is slightly higher than that given in the literature (852.7 eV),[17] suggesting the possibility of the presence of Re-Ni in addition to metallic Ni, as supported by the fitting of the Re 4f spectrum.

Although the Ni $2p_{3/2}$ peak position of Ni_2O_3 is pretty close to that of $Ni(OH)_2$,[20,22,23] its presence should be excluded on the following grounds: Ni_2O_3 cannot be obtained as a result of cathodic reduction, but rather appears to be due to atmospheric oxidation. As such, its content should not decrease with deposition time. On the contrary, the content of the component at 856.3 eV is strongly decreased with

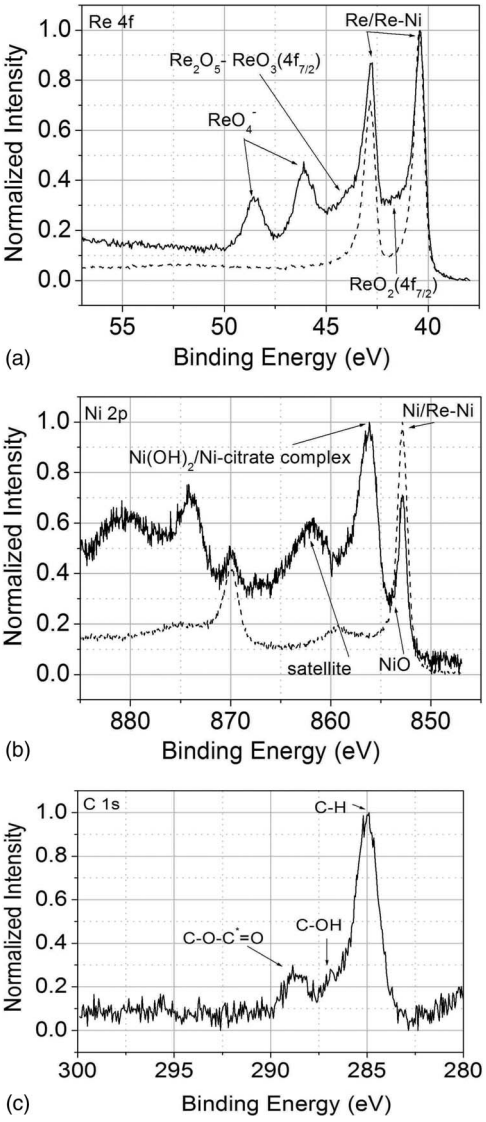

Figure 4. HR-XPS spectra of Re-Ni film deposited at 50 mA cm^{-2} and 70°C for 10 s. Re 4f, solid line – before sputtering, dashed line – after sputtering. For Re, Re-Ni and ReO_4^-, both Re $4f_{7/2}$ and Re $4f_{5/2}$ peaks are marked with arrows, while for other components – only the Re $4f_{7/2}$ peak position is marked. (b) Ni 2p, solid line – before sputtering, dashed line – after sputtering. Component assignment is given for the Ni $2p_{3/2}$ peaks only. (c) C 1s, before sputtering.

deposition time (cf. Table II), excluding its attribution to Ni_2O_3. The data presented in Tables II and III clearly demonstrate changes in composition with deposition time, showing the growth in metallic and intermetallic species with simultaneous reduction of highly oxidized

Table II. The effect of the deposition time on the content of different components before sputtering, as determined from HR-XPS, Ni $2p_{3/2}$ data curve-fitting.

	Binding energy of fitted Ni $2p_{3/2}$ component and its content in %		
Deposition time (s)	Ni / Re-Ni	NiO	$Ni(OH)_2$/Ni–citrate complexes
5	853.07 eV	854.11 eV	856.30 eV
	8.5%	4.6%	86.9%
10	852.87 eV	853.91 eV	856.30 eV
	24.3%	3.5%	72.2%
20	852.87 eV	853.91 eV	856.10 eV
	37%	5.9%	57.1%
300	853.02 eV	854.11 eV	856.30 eV
	60.6%	9.7%	29.7%

Table III. The effect of deposition time on the content of different components before sputtering, as determined from HR-XPS Re 4f data curve-fitting.

		Binding energy of fitted Re 4f component and its content in % at					
Deposition time (s)	components	Re	Re-Ni	ReO_2	Re_2O_5	ReO_3	ReO_4^-
10	$4f_{7/2}$	40.44 eV	41 00 eV	42.00 eV	43.50 eV	44.60 eV	46.13 eV
	$4f_{5/2}$	42.87 eV	43.43 eV	44.43 eV	45.93 eV	47.03 eV	48.56 eV
		34.1%	16.7%	18.1%	5.9%	2.6%	22.7%
20	$4f_{7/2}$	40.44 eV	41 00 eV	42.00 eV	43.50 eV	44.60 eV	46.03 eV
	$4f_{5/2}$	42.87 eV	43.43 eV	44.43 eV	45.93 eV	47.03 eV	48.46 eV
		36.8%	18.0%	19.6%	6.4%	2.8%	16.4%
300	$4f_{7/2}$	40.30 eV	41 00 eV	42.00 eV		44.60 eV	45.93 eV
	$4f_{5/2}$	42.73 eV	43.43 eV	44.43 eV	Absent	47.03 eV	48.36 eV
		50.5%	34.4%	7.1%		2.7%	5.3%

components. The content of Ni/Re-Ni is strongly increased along with increase in deposition time, while the content of NiO is rather low and is increased mostly for the longest time of deposition. Experimentally we find that the content of $Ni(OH)_2$ and/or nickel citrate complexes decreased with deposition time (cf. Table II). The content of Re/Re-Ni is increased, while that of ReO_4^- is decreased substantially with deposition time. The content of ReO_3 is rather low (2.6–2.8%) and almost constant. At 20 s deposition time, the contents of ReO_2 and Re_2O_5 are slightly higher than at 10 s. At 300 s the content of ReO_2 is almost 3 times lower and no Re_2O_5 is observed (Table III).

To summarize, the results presented in Tables II and III indicate changes in the surface composition of the film with deposition time – the concentrations of ReO_4^- and Ni-Cit decrease while the concentrations of Ni, Re and Re-Ni increase. The noticeable decrease in ReO_4^- and Re_2O_5 concentrations as well as the increase in NiO concentration were observed at a rather long time (300 s). The changes in composition of the film surface layer reflect the changes in composition of the interface between the growing film (cathode) and the electrolyte and can explain the changes in the catalytic activity of the cathode surface. No oxides were found inside the films after surface sputter cleaning (Figs. 4a,4b).

Typical HR-XPS C 1s spectrum of the Re-Ni surface before sputtering is presented in Fig. 4c. The spectrum contains the components attributed to alcohol and ester-derived species. The same components were observed on the surface of Pt cathodes after sodium citrate electrolysis and were shown to be the result of citrate decarboxylation.[24]

***The electrodeposition process.*—**In this section we consider the mechanism of the process suggested before[13,14] and its agreement with the results of the present investigation. As pointed out before,[6–8] catalysis by freshly deposited Ni can explain the induced codeposition of Re and regularities of the process at long deposition times, i.e. at the scale of tens of minutes. However, this concept cannot explain the effects observed at the early stages of deposition. These effects include the enhancement of both Ni^{2+} and ReO_4^- reduction that are present in the citrate electrolyte, the decrease of the AFE (i.e. fading of the chemical reaction), and the decrease of Re content in the deposits with deposition time. Exclusion of one of the components of the electrolyte causes the disappearance of all above effects. Explanation of these phenomena is possible in terms of a catalytic electrode surface that enhances reduction of both Re and Ni and is changed with deposition time.[13,14]

Taking into account the deformation of the ReO_4^- anion in the presence of a Ni-Citrate complex in the electrolyte, as shown by Raman spectroscopy, we proposed the existence of a precursor that consists of both the deformed ReO_4^- and the Ni-Cit complex. Facilitated reduction of Re and Ni from this precursor presumably leads to formation of a catalytic layer composed of the products of their reduction (including intermediates). Additionally, the Re-Ni alloy deposition process includes catalytic deposition of Re from ReO_4^- and Ni from Ni-Cit complex on the surface of the catalytic layer. Thus, we believe that at least 3 parallel routes of reduction exist:

(1) Re-Ni from ReO_4^-/Ni-Cit precursor
(2) Ni from Ni-Cit
(3) Re from ReO_4^-

Process (1) is facilitated by the mutual deformation of ReO_4^- and Ni-Cit in precursor. Processes (2) and (3) are catalyzed by the products of process (1).

It could be expected that the deposits produced by deposition from the general precursor consist of bonded (alloy) Re-Ni species, while parallel deposition from Ni-Cit and ReO_4^- separately yields separate Re and Ni species. Based on correlative APT and STEM data,[15] we have recently concluded that Ni is actually codeposited as an element of a binary alloy.

The results of SIMS and XPS obtained in the present work are in agreement with the discussion above. The presence of Re-Ni, Re-Ni-O_x (Re-Ni-O, Re-Ni-O_2) and C_2H_4-O-Re-Ni on the surface and the presence of Re-Ni in the bulk indicate a notable interaction between Ni and Re in the Re-Ni deposits. Separate Re and Ni species were also found. Although such interaction cannot be considered as a definite evidence of the simultaneous deposition from a precursor containing ReO_4^- and $(NiCit)^-$ or $(NiCit)^{4-}$ complex, it can support indirectly this idea. The formation of a multilayer Re–Ni structure has been related to the Re–Ni binary phase diagram—a peritectic phase diagram with an extensive region of mutual solubility and no intermetallic compounds—and to alternate depletion and enrichment of nickel ions in the diffusion layer.[15] When a Re-rich layer forms, more hydrogen is being formed due to the catalytic effect of Re on the hydrogen evolution reactions. Consequently, the pH is increased locally, thus favoring the formation of a nickel hydroxide intermediate at the surface of the cathode. Hydrogen evolution can also result in more nickel ions in the diffusion layer due to increased convection. When a Ni-rich layer forms, less hydrogen is evolved, the local pH decreases, and a new cycle begins. The bands of the Re-rich phase are thicker than the bands of the Ni-Rich phase because the depletion of nickel ions in the diffusion layer is less significant than the depletion in perrhenate ions.[15] The periodic compositional modulations observed in the SIMS profiles are in agreement with our previous STEM and APT data.

In order to explain the high values of the AFE, we have to accept the occurrence of a chemical reaction, with participation of some reducing agent. As shown above, the SIMS data confirm the declining Re content in the film with deposition time (Fig. 2) and the concept of a chemical reaction occurring at the initial stages of deposition and fading with deposition time (Fig. 3 and Table I). The only reducing agent in our system is citric acid. The processes of synthesis of Au, Pt and Ag nano-particles by chemical reduction with citrate are common.[25–28] The first stage of these processes is believed to be the decarboxylation of citrate on Au catalytic surface and formation of acetone-1, 3-dicarboxylate according to the following Scheme 1:[26]

$$\left(^-OCOCH_2\right)_2C\left(OH\right)OCO^- \rightarrow \left(^-OCOCH_2\right)_2CO + CO_2 + H^+ + 2e^-$$

Scheme 1.

Recently, data were obtained in favor of the pathway including the formation of Au^{3+}-Cit complex, transformation of its structure to that allowing metal–ligand electron transfer, and reduction of Au^{3+} by citrate accompanied by its decarboxylation.[29] A similar mechanism of intramolecular transfer of electrons from citrate to the metal with variable valence in the complex was shown to be involved in the decomposition of Mn^{3+}-Cit complex with reduction of Mn^{3+} to Mn^{2+} by citrate,[30] and in the catalytic reduction of Cr^{6+} to Cr^{3+} by citrate in the presence of Mn^{2+}, Cu^{2+} or Fe^{3+}.[31–33] Electron transfer inside citrate complexes with Mn^{2+}, Cu^{2+} or Fe^{3+} causes the formation of organic acid radicals, CO_2 and O_2 radicals leading to a rapid reduction of Cr^{6+} to Cr^{3+}.

We cannot exclude the possibility of intramolecular charge transfer in the deformed Ni-Cit complexes initiated by the potential shift in the negative range. As shown in our earlier work,[13] the chemical process was triggered only by application of current and was more intensive at higher current densities. No chemical process was observed at open circuit or in the absence of citric acid in the electrolyte. Initiation of Ni-Cit complex by the potential shift is similar to photo-initiation of the catalytic reduction of Cr^{6+} by citrate in the presence of Cu^{2+} or Fe^{3+}.[32,33] The decrease of concentrations of Ni-Cit and ReO_4^- on the cathode surface with deposition time shown by HR-XPS analysis (Tables II and III) is in agreement with this concept of catalysis of the chemical process.

Oxides such as ReO_3, Re_2O_5, ReO_2 and NiO, which are present on the surface of the deposits, can also be involved in catalytic decomposition of citrate as well as in the catalysis pathway of Re and Ni electrodeposition in processes (2) and (3) above. This statement is justified by the fact that oxides of Ni and Re are known catalysts for different chemical and electrochemical reactions. In many cases the catalytic activity of the mixed oxides is higher than that of each of them separately.[34–36] The changes of the Re_2O_5, ReO_2 and NiO concentrations with deposition time (Tables II and III) can also be responsible for the changes of catalytic activity of the cathode.

The catalytic properties of the cathodic surface during Re-Ni deposition toward decarboxylation of citrate is confirmed by the fact that the comparable intensities of the HR-XPS C 1s spectra on Pt[24] and Re-Ni cathode surfaces (Fig. 4c) were obtained after electrolysis for 0.5–2.0 h and 5–10 s, respectively.

It should be noted that the process of Re-Ni induced codeposition is very complicated. Although the data obtained in the course of this work by means of SIMS and HR-XPS are consistent with those obtained by electrochemical experiments,[13,14] and with the suggested catalytic mechanism of induced codeposition, at the present level of our knowledge we cannot determine the catalytic pathway of both chemical and electrochemical reactions.

Conclusions

In this work we used TOF-SIMS and HR-XPS to characterize the chemical composition and oxidation states of Re-Ni alloys electrodeposited at short deposition times of 2–300 s, in an attempt to better understand the mechanism of induced-codeposition in this sysem. TOF-SIMS and HR-XPS results indicate a notable interaction between Ni and Re in the Re-Ni deposits, and indirectly support deposition from a precursor containing Ni^{2+}, ReO_4^- and citrate species. The TOF-SIMS results confirm the high deposition rates and the corresponding Anomalous Faradaic Efficiency (AFE) at short deposition times, as well as the decrease of the AFE and Re content in deposits with increasing deposition time. Our observations support a concept of chemical reduction proceeding in parallel with electrochemical reduction in the initial stages of deposition. HR-XPS demonstrates the changes in the deposit surface composition with deposition time, showing the growth in metallic and intermetallic species with simultaneous reduction of highly oxidized components. The directed compositional changes at the cathode surface with deposition time are believed to lead to the decrease in the catalytic activity of the cathode toward a chemical reaction and its fading with deposition time. The results of the present work are in agreement with the results of our previous studies and with the concept of a catalytical mechanism in the initial stages of Re-Ni codeposition. However, it should be noted that the process is not yet completely proven.

Acknowledgments

Partial funding by the U.S Air Force Office of Scientific Research (AFOSR grant #FA9550-10-1-0520) and the Israel Department of Defense (#4440258441) is greatly appreciated.

References

1. E. Eliaz and E. Gileadi, in *Modern Aspects of Electrochemistry*, Editors: C.G. Vayenas, R.E. White, and M.E. Gamboa-Aldeco, Springer, Vol. **42**, 191 (2008).
2. L. E. Netherton and M. L. Holt, *J. Electrochem. Soc.*, **98**, 106 (1951).
3. H. Fukushima, T. Akiyama, Y. Toyoshima, and K. Higashi, *J. Met. Finish. Soc. Jpn.*, **36**, 198 (1985).
4. T. Jones, *Metal Finishing*, **6**, 86 (2003)
5. P. R. Zabinski, A. Franczak, and R. Kowalik, *ECS Trans.*, **41**, 39 (2012).
6. A. Naor, E. Eliaz, and E. Gileadi, *Electrochim. Acta*, **54**, 6028 (2009).
7. A. Naor-Pomeranz, L. Burstein, N. Eliaz, and E. Gileadi, *Electrochem. Solid-State Lett.*, **13**, D91 (2010).
8. A. Naor, E. Eliaz, and E. Gileadi, *J. Electrochem. Soc.*, **157**, D422 (2010).
9. B. A. Rosen, E. Gileadi, and N. Eliaz, *J. Electroanal. Chem.*, **731**, 93 (2014).
10. O. Younes and E. Gileadi, *J. Electrochem. Soc.*, **149**, C100 (2002).
11. O. Younes-Metzler, L. Zhu, and E. Gileadi, *Electrochim. Acta*, **48**, 2251 (2003).
12. N. Eliaz, T. M. Sridhar, and E. Gileadi, *Electrochim. Acta*, **50**, 2893 (2005).
13. O. Berkh, N. Eliaz, and E. Gileadi, *J. Electrochem. Soc.*, **161**, D219 (2014).
14. O. Berkh, A. Khatchatouriants, N. Eliaz, and E. Gileadi, *J. Electrochem. Soc.*, **161**, D632 (2014).
15. S. -I. Baik, A. Duhin, P. J. Phillips, R. F. Klie, E. Gileadi, D. N. Seidman, and N. Eliaz, *Adv. Eng. Mater.* (2016).
16. K. J. Kim, D. Simons, and G. Gillen, *Appl. Surf. Sci.*, **253**, 6000 (2007).
17. J. F. Moulder, W. F. Stickle, P. E. Sobol, and K.D. Bomben, *Handbook of X-ray Photoelectron Spectroscopy*, Perkin-Elmer Corp., p. 235 (1992).
18. A. Cimino, B. A. De Angelis, D. Gazzoli, and M. Z. Valigi, *Anorg. Allg. Chem.*, **460**, 86 (1980).
19. T. Dickinson, A. F. Povey, and P. M. A. Sherwood, *J. Chem. Soc. Faraday Trans.*, **1**, 327 (1977).
20. P. Prieto, V. Nistor, K. Nouneh, M. Oyama, M. Abd-Lefdil, and R. Diaz, *Appl. Surf. Sci.*, **258**, 8807 (2012).
21. P. Dufresne, E. Payen, J. Grimblot, and J. P. Bonnelle, *J. Phys. Chem.*, **85**, 2344 (1981).
22. L. Salvatl, L. E. Makovsky, J. M. Stencel, F. R. Brown, and D. M. Hercules, *J. Phys. Chem.*, **85**, 3700 (1981).
23. K. Kishi, *J. Electron Spectrosc. Relat. Phenom.*, **46**, 237 (1988).
24. O. Berkh, L. Burstein, Y. Shacham-Diamand, and E. Gileadi, *J. Electrochem. Soc.*, **158**, F85 (2011).
25. P. L. Redmond, X. Wu, and L. Brus, *J. Phys. Chem. C* **111**, 8942 (2007).
26. S. Kumar, K. S. Gandhi, and R. Kumar, *Ind. Eng. Chem. Res.* **46**, 3128 (2007).
27. P. Zhao, N. Li, and D. Astruc, *Coord. Chem. Rev.* **257**, 638 (2013).
28. P. R. van Rheenen, M. J. McKelvy, and W. S. Glaunsingers, *J. Solid State Chem.* **67**, 151 (1987).
29. I. Ojea-JimeFnez and J. M. Campanera, *J. Phys. Chem. C*, **116**, 23682 (2012).
30. J. K. Klewicki and J. J. Morgan, *Environ. Sci. Technol.* **32**, 2916 (1998).
31. B. Sarkar, R. Naidu, G. Sr. Krishnamurti, and M. Megharaj, *Environ. Sci. Technol.* **47**, 13629 (2013).
32. Y. Li, Ch. Chen, J. Zhang, and Y. Lan, *Chemosphere* **127**, 87 (2015)
33. Z. Xu, Sh. Bai, J. Liang, L. Zhou, and Y. Lan, *Mater. Sci. Eng. C*, **33**, 2192 (2013).
34. K. Chayakul, T. Srithanratana, and S. Hengrasmee, *Catal. Today*, **175**, 420 (2011).
35. J. Landon, E. Demeter, N. İnoğlu, C. Keturakis, I. E. Wachs, R. Vasic, A. I. Frenkel, and J. R. Kitchin, *ACS Catal.* **2**, 1793 (2012).
36. V. P. Pashova, L. G. Mirkova, M. H. Monev, P. Nowak, and G. Nawrat, *Bulg. Chem. Commun.* **43**, 64 (2011).